High-Throughput Screening

International Edition: DOI: 10.1002/anie.201609655
German Edition: DOI: 10.1002/ange.201609655

Small Molecule Microarray Based Discovery of PARP14 Inhibitors

Bo Peng, Ann-Gerd Thorsell, Tobias Karlberg, Herwig Schüler, and Shao Q. Yao**

Abstract: *Poly(ADP-ribose) polymerases (PARPs) are key enzymes in a variety of cellular processes. Most small-molecule PARP inhibitors developed to date have been against PARP1, and suffer from poor selectivity. PARP14 has recently emerged as a potential therapeutic target, but its inhibitor development has trailed behind. Herein, we describe a small molecule microarray-based strategy for high-throughput synthesis, screening of >1000 potential bidentate inhibitors of PARPs, and the successful discovery of a potent PARP14 inhibitor* ***H10*** *with >20-fold selectivity over PARP1. Co-crystallization of the PARP14/****H10*** *complex indicated* ***H10*** *bound to both the nicotinamide and the adenine subsites. Further structure–activity relationship studies identified important binding elements in the adenine subsite. In tumor cells,* ***H10*** *was able to chemically knockdown endogenous PARP14 activities.*

Poly(ADP-ribose) polymerases, or PARPs, are ADP-ribosylating enzymes that comprise at least 18 members in humans.[1] During ribosylation, the enzymatically activated PARP uses nicotinamide adenine dinucleotide (NAD^+) as a co-substrate to transfer ADP-ribose to its targets while releasing nicotinamide as the metabolized product (Figure 1 A). Amongst the PARP family members, most research has thus far focused on PARP1, an enzyme that is critically involved in DNA repair and participates in a variety of cellular functions. Consequently, many potent PARP1 inhibitors, including some FDA-approved drugs (such as Olaparib in Figure 1 A), have been successfully developed.[2,3] The other PARP family members, especially the mono(ADP-ribosyl) transferases (*m*-ARTs), have remained poorly characterized, in large part due to a lack of cell-permeable small molecule inhibitors.[3] Emerging evidence suggests important cellular functions for some of these enzymes. For instance PARP14, an *m*-ART, was found to be associated with the development of inflammatory diseases and various types of cancer.[4,5] In recognition of the urgent need to develop small molecule inhibitors against PARP14 and other less-studied PARPs,[3,6,7] we report herein a small molecule microarray (SMM)-based strategy suitable for high-throughput synthesis and screening of potential bidentate inhibitors of PARPs, and the successful discovery of a cell-permeable inhibitor, **H10** (Figure 1 B), that showed relatively potent in vitro inhibitory activity against PARP14 ($IC_{50} = 490$ nM) with good selectivity over other PARPs (≈24-fold over PARP1). A crystal structure of the PARP14/**H10** complex revealed that **H10** is the first bidentate inhibitor against an *m*-ART, binding to both the nicotinamide and adenine subsites of PARP14. Subsequent medicinal chemistry efforts provided valuable structure–activity relationship (SAR) on **H10** analogues interacting with residues in the adenine-binding site of PARP14. Lastly, in cellulo studies of selected inhibitors with tumor cells indicated the compounds conferred moderate cellular PARP14 knockdown activities.[4,5]

Most known PARP inhibitors are structural mimics of the nicotinamide moiety in NAD^+ (Figure 1 A), which inevitably leads to poor selectivity amongst the PARP family members due to their highly conserved NAD^+-binding pockets.[3,8] Olaparib, for instance, has been shown to display non-selective binding against PARP1, 2, 3, and 4.[3] Deviating from our previous strategy to develop PARP1-selective inhibitors by targeting the BRCT (BRCA1 C-terminus) domain, which is present only in PARP1 and PARP4,[9] our new strategy aimed to explore possible secondary binding sites in PARP14 and other PARPs, that is, the target-binding site and/or the adenine-binding subsite located next to the nicotinamide binding pocket (Figure 1 A).[3] We reasoned that, due to different functions (for example, mono- vs. poly-ADP-ribosylation) as well as various targets modified by PARPs, such binding sites (or subsites) might be structurally distinct. A bidentate inhibitor capable of making contacts with both the primary nicotinamide-binding site and a secondary binding site, if tethered with a suitable linker, should possess improved binding affinity and specificity for potential targeting of individual PARP proteins. In fact, bidentate inhibitors of kinases and phosphatases, which also possess multiple binding pockets, are known.[10,11] Recently reported inhibitors of human tankyrases (TNKS1/2, a member of the PARP subfamily), also showed binding to both the nicotinamide and adenine subsites.[12]

With the above considerations, we devised a strategy to design, synthesize, and identify PARP bidentate inhibitors. Previously, we and others used Cu^I-catalyzed azide–alkyne cycloaddition (CuAAC) for the rapid synthesis and screening of bidentate inhibitors against different enzymes.[13,14] While this method is a step forward compared to traditional compound synthesis/screening strategies, it is time-consuming, resource-intensive, and often complicated by the risk of compound impurities. Small molecule microarrays (SMMs) are miniaturized assemblies of compounds immobilized across a 2.5×7.5 cm glass slide, on which thousands of protein–ligand interactions may be simultaneously measured.[15,16] Over the years, by improving key aspects related

[*] B. Peng, Prof. Dr. S. Q. Yao
Department of Chemistry
National University of Singapore
3 Science Drive, Singapore 117543 (Singapore)
E-mail: chmyaosq@nus.edu.sg
A.-G. Thorsell, Dr. T. Karlberg, Dr. H. Schüler
Karolinska Institute
Department of Medical Biochemistry & Biophysics
Scheeles väg 2, 17177 Stockholm (Sweden)
E-mail: herwig.schuler@ki.se

Supporting information for this article can be found under: http://dx.doi.org/10.1002/anie.201609655.

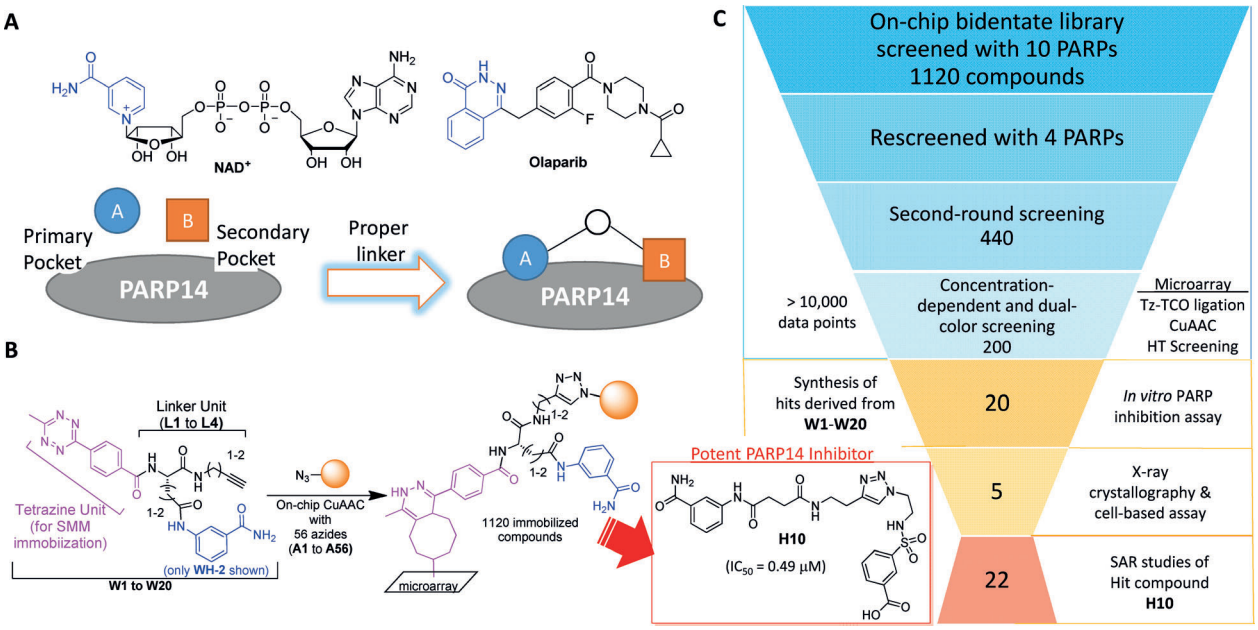

Figure 1. A) Chemical structure of NAD^+ and Olaparib (top). Bottom) Scheme showing a bidentate inhibitor upon binding to both the primary and secondary pockets PARP14 with a suitable linker. B) Scheme showing our microarray-based discovery of PARP14 inhibitors. Trifunctional compounds (**W1**–**20**) were spotted on TCO slides, followed by on-chip CuAAC with azides (**A1**–**56**) to generate the corresponding SMM containing 1120 bidentate PARP inhibitors. Subsequent SMM screening led to identification of a potent PARP14 inhibitor **H10**. C) Overall workflow of the current study, including SMM screening, solution-phase resynthesis, and in vitro screening, X-ray studies of **H10**/PARP14 complex, structure-based medicinal chemistry, and cell-based hit validation.

to immobilization,[16b] on-chip quantitative binding measurements, and dual-color fluorescence screening,[9,16a,d] we have successfully used this technology for rapid screening and identification of small molecule inhibitors against a variety of targets.[16] Inspired by recent work in which on-chip CuAAC was used to assemble a carbohydrate-based compound library,[17] our current study made use of a similar strategy (Figure 1 B,C); by using tetrazine (Tz)-*trans*-cyclooctene (TCO) ligation to rapidly print 20 alkyne-containing trifunctional compounds (**W1** to **W20**; Table S1) into each well of a 12-well glass slide, followed by CuAAC coupling with 56 different azides (**A1** to **A56**; Table S2), an 1120-membered SMM was rapidly generated with minimal compound consumption. The Tz-TCO ligation was previously shown to allow rapid and highly efficient compound immobilization in a microarray.[16b] With the nearly quantitative yield of a typical CuAAC coupling, we expected most if not all of the 1120 bidentate inhibitors to be successfully assembled on the microarray. An additional advantage of this strategy was that purification of immobilized compounds could be done en masse by simple washes of the resulting microarray to remove contaminating CuAAC reagents/copper catalysts, as well as excessive azides, all of which are known to cause severe interference during screening with compounds synthesized from solution-phase CuAAC methods.[13,14]

As shown in Figure 1 B and Scheme S1, **W1**–**20** were synthesized from five different ligands known to bind to the nicotinamide-binding pocket of PARP1 (**WH-1** to **WH-5**), and they were expected to bind well to other PARP proteins. The Tz moiety was attached to these ligands through four different linkers derived from aspartic/glutamic acids attached to amine-containing terminal alkynes (**L1** to **L4**). These linkers were chosen on the basis of their flexibility, length, and easy chemical access, so as to better exploit the altered distances between the primary and secondary binding pockets of different PARPs. The 56 different azides (**A1**–**56**) were synthesized by using a previously published protocol,[18] with common aliphatic/aromatic amines containing diverse functional groups. We also included compounds derived from known kinase inhibitors (Scheme S1); because many kinase inhibitors are structural mimics of adenine, our chosen azides, if properly tethered to the primary pocket-binding anchors (**WH-1** to **WH-5**), might preferentially fit into the secondary pocket of different PARPs, resulting in an overall increase of the bidentate inhibitor binding affinity and selectivity.

The successful immobilization of **W1**–**20** to Tz-functionalized slides followed by subsequent on-chip CuAAC with azides was confirmed by spotting a tetrazine-containing dye (TER-Tz) and coupling a control well on the spotted microarray with TER-N_3 (Figure 2 A). To construct the 1120-membered SMM, a total of five 12-well spotted microarrays were used, with each well coupled to one azide. The entire on-chip CuAAC synthesis was completed in one overnight reaction including post-SMM compound purification by washing. With the SMM in hand, preliminary microarray screenings were first carried out with 10 fluorescently labeled recombinant PARP catalytic domain proteins (Figures 1 C, S1–S9). In total, >10000 data points were generated in a single screening experiment. Upon microarray data analysis, we obtained high-quality bidentate-binding microarray images against four of the PARPs (TNKS1, TNKS2, PARP10, and PARP14). For the other six PARPs (PARP1,

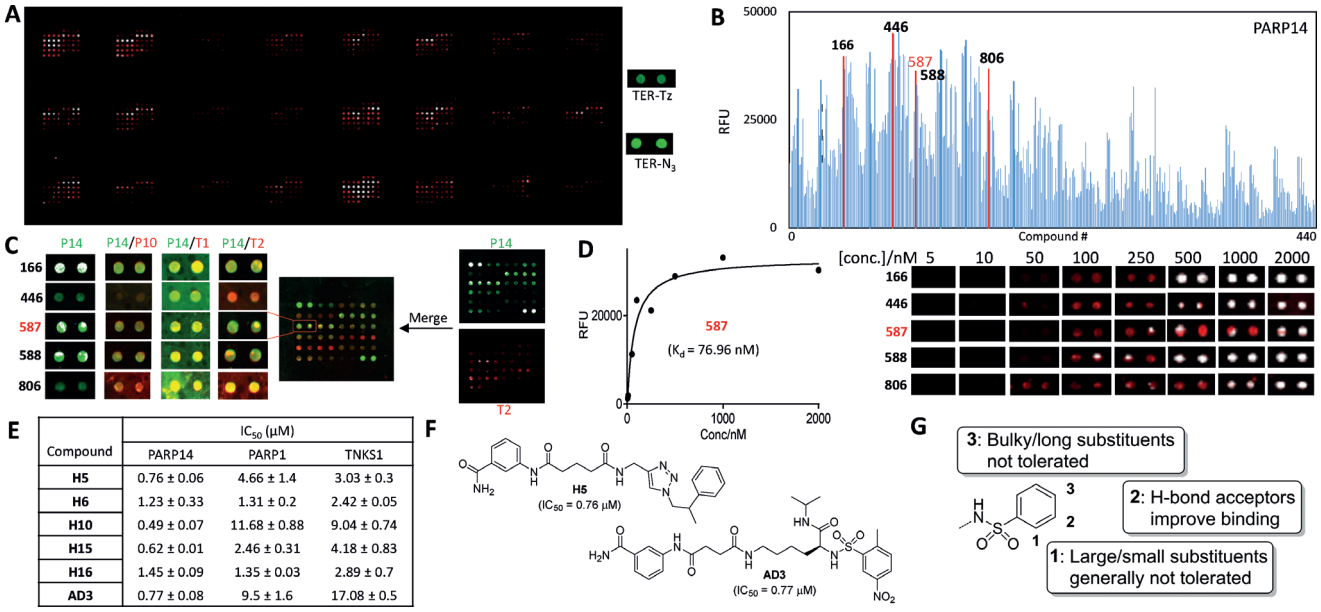

Compound	IC_{50} (μM)		
	PARP14	PARP1	TNKS1
H5	0.76 ± 0.06	4.66 ± 1.4	3.03 ± 0.3
H6	1.23 ± 0.33	1.31 ± 0.2	2.42 ± 0.05
H10	0.49 ± 0.07	11.68 ± 0.88	9.04 ± 0.74
H15	0.62 ± 0.01	2.46 ± 0.31	4.18 ± 0.83
H16	1.45 ± 0.09	1.35 ± 0.03	2.89 ± 0.7
AD3	0.77 ± 0.08	9.5 ± 1.6	17.08 ± 0.5

Figure 2. A) Microarray image of the 440-membered SMM screened with fluorescently labeled PARP14. All of the compounds were spotted in duplicate. Right) Images of spots showing successful immobilization of TER-Tz on TCO slides and on-chip CuAAC with TER-N_3. B) Histogram showing the relative fluorescence (RFU) of each compound from the SMM in (A). Red: Representative hits. See decoding table (SI_II) for IDs and structures. C) Dual-color results of representative hits simultaneously screened with PARP14 (green) and another PARP (red; PARP10, TNKS1, or TNKS2). D) Microarray images of spots from concentration-dependent SMM and a representative K_d curve. E) Data summarizing IC_{50} values obtained from in vitro PARP assay against 5 resynthesized hits. F) Structures of two PARP14 inhibitors, **H5** and **AD3**. G) SAR of the adenine-binding site summarized from X-ray and medicinal chemistry studies.

2, 3, 4, 12, and 13), the S/N ratios of the fluorescent spots were on average 5- to 10-fold lower, and were deemed unreliable for subsequent screening/compound identification (Figure S3). They were therefore not pursued further. The next several rounds of microarray screening involved: 1) rescreening of the 1120-membered SMM with the 4 selected PARPs (Figures S3 and S4); 2) second-round screening with a 440-membered focus microarray spotted with compounds deemed as "positive binders" from the previous round (Figure S5); and 3) third-round screening of selected compounds with dual-color and concentration-dependent experiments (Figures S6–8). Dual-color microarray screening, in which spotted compounds were screened on the same slide with two different fluorescently labeled protein targets (Cy3-labeled PARP14 and a Cy5-labeled control), enabled rapid identification of compounds having highly selective binding of one protein over another.[16a] Concentration-dependent microarray experiments allowed all spotted compounds to be simultaneously screened in a single platform with different concentrations of a protein, thus providing semi-quantitative binding data (apparent K_d) for rapid and accurate identification of high-affinity ligands.[16d] A representative second-round microarray image obtained from the 440-membered focus SMM screened against Cy3-labeled PARP14 and its corresponding histogram showing the relative fluorescence intensity (RFU) of individual spots are shown in Figure 2A and B, respectively. In Figure 2B, representative high-fluorescence spots were colored and numbered (according to the SI II decoding table). Microarray images of the corresponding compounds rescreened in the third round are shown in Figure 2C and D. Because we were particularly interested in the discovery of potential PARP14 inhibitors, the dual-color experiments were carried out with a 1:1 mixture of Cy3-labeled PARP14 and another Cy5-labeled PARP protein (PARP10, TNKS1, and TNKS2, respectively). Merged images of the two resulting fluorescence channels (colored in green and red, respectively, in Figure 2C) allowed immediate visual identification of PARP14-selective ligands. For example, spots derived from compound **587** appeared mostly green across the various dual-color images, indicating it was a putative PARP14-selective binder. Similarly, in concentration-dependent experiments (Figure 2D), the same compound showed PARP14 dose-dependent binding profiles with an apparent on-chip K_d of 76.96 nM, indicating it was a high-affinity PARP14 ligand. In total, 20 putative PARP14 ligands were identified from three rounds of microarray screenings (Table S3). In addition to compound **587**, results from four other compounds (**166**, **446**, **588**, **806**) are shown in Figure 2B/C/D. All 20 of the putative hits possessed either high-binding affinity or selectivity toward PARP14, or both. Interestingly, all contained the same 3-amino-benzamide moiety (**WH2**), which was derived from a previously reported but relatively weak PARP1 inhibitor.[19]

Our next-step screening efforts involved in vitro PARP enzymatic assays to evaluate these 20 hits against several PARP proteins (PARP1, PARP14, and TNKS1; Figures 2E, S11, and S12). Because the tetrazine immobilization unit was no longer required, the 20 hits derived from tetrazine-free **W1**–**W20** (renamed as **H1** to **H20**; Table S3), containing either a succinic or glutaric acid linker (to minimize molecular weight and maximize flexibility of the linker), were resynthesized. Structures of two examples, **H10** and **H5** (correspond-

ing to compounds **587** and **166** in the microarray, respectively) are shown in Figures 1B and 2F. **H10** was found to inhibit PARP14 activity with an IC_{50} value of 0.49 ± 0.07 μM in vitro, which represents the most potent PARP14 inhibitor reported to date.[6,7,20] Equally important, it also possessed relatively good selectivity over two other PARPs tested (24- and 18-fold over PARP1 and TNKS1, respectively). **H5**, the next-best PARP14 inhibitor identified ($IC_{50} = 0.76 \pm 0.06$ μM), showed a comparatively poorer selectivity over PARP1 (≈6-fold).

To determine the structural basis of PARP14 binding to **H10**/**H5**, we next obtained X-ray structures to resolutions of 2.17 Å (for **H10**) and 2.07 Å (for **H5**), respectively. As shown in Figure 3, the PARP14/**H10** complex clearly showed the 3-

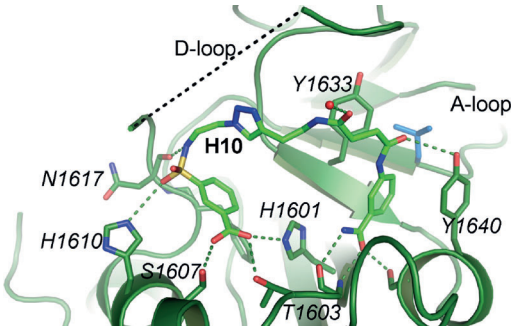

Figure 3. Close-up view of the **H10**-binding site in the X-ray structure of PARP14/**H10** complex (PDB entry 5LYH). **H10** and PARP14 are shown in ball and sticks, and ribbons, respectively.

amino-benzamide moiety from **H10** resided in the nicotinamide (NA)-binding pocket as expected, and the rest of the molecule extended toward the adenine-binding site in a binding mode that was not observed previously.[3] The sulfonamide and benzoic acid moiety at the distal end were found in the adenine base-binding site of PARP14. Both the linker and distal end made a number of polar interactions (notably, with PARP14 side chains His1682, Thr1684, Ser1688, His1691, and the peptide backbone of Asn1698) that could explain the slightly improved potency and the significantly better selectivity of the compound. Extending the central linker in **H10** by one carbon (giving **H15**; Table S3) decreased both potency and selectivity. Surprisingly, the second crystal structure shows that **H5** bound to PARP14 in a different fashion (Figure S13); its distal phenyl group made hydrophobic interactions with the Val1773 and Val1784 side chains in a site around the small hydrophobic residue that characterizes the mono-ADP-ribosyltransferases of the PARP family, Leu1782.[3] This was an interesting observation because binding at the subsite near the A-loop might provide a means to accomplish truly selective inhibition even within the mono-ADP-ribosyltransferases.[21] Notwithstanding, our PARP14/**H10** structure clearly showed that, by using the bidentate strategy, selective PARP14 inhibitors could be generated by engaging a 3-sulfonamide benzoic acid in the adenine binding site.

Owing to incomplete density of the flexible D-loop in our PARP14/**H10** structure, this segment could not be completely modeled. We wondered, by engaging the unresolved D-loop, whether specific interactions might be introduced in the linker region of **H10** to improve its PARP14-binding affinity. Medicinal chemistry efforts were thus carried out (Figure 2G, Scheme S3, and Table S4). By first substituting the triazole-containing linker in **H10** with more flexible linkers containing piperazine, ethylene glycol, or lysine, we found most of the resulting inhibitors, except the lysine-containing **H10** analogue (**18** in Scheme S3), had attenuated PARP14 inhibition. This inhibitor was thus chosen for further SAR studies. We focused on the adenine-binding subsite in which numerous interactions between the 3-sulfonamide benzoic acid of **H10** and PARP14 were observed (Figure 3). The NH in SO_2NH formed a hydrogen bond with Asn1698 of the protein, while its O formed another hydrogen bond with His1691. In addition, the benzoic acid group also formed several favorable interactions with the protein. A 22-membered arylsulfonamide library based on **H10** was thus synthesized (named **AD1** to **AD22**; Table S4) and tested for PARP14 inhibition (Figure S11C) with results summarized in Figure 2G. Most of the compounds except **AD3** (Figure 2F) showed attenuated inhibition. Nevertheless, SAR analysis indicated, as predicted from the crystal structure, that while large substituents in C1/C3 of the arylsulfonamide were not tolerated, hydrogen bond-accepting C2 substituents might improve ligand binding.

Finally, we evaluated whether **H10** and **AD3** could inhibit endogenous PARP14 activities from tumor cells. Both compounds showed good cell permeability (Table S6) and hydrolytic stability (Figure S15).[16c] Because the majority of poly(-ADP-ribosyl)ation (PAR) activity in mammalian cells is from PARP1, we first assessed whether our newly discovered PARP14 inhibitors cross-inhibited endogenous PARP1 activity. We treated HepG2 cells (a liver cancer cell line) with H_2O_2 to induce DNA damage and oxidative stress leading to PAR polymer formation (Figure 4A).[9] Addition of PARP1 inhibitors such as DPQ or Olaparib, but not **H10** or **AD3** (even at 25 μM), caused apparent inhibition of PAR formation, indicating neither **H10** nor **AD3** inhibited endogenous PARP1 activities. It was previously reported that PARP14 promotes tumor survival in multiple myeloma and hepatocellular carcinoma by blocking the c-Jun N-terminal kinase 1 (JNK1)-mediated cell apoptosis.[4,5] Genetic knockdown of endogenous PARP14 expression could thus lead to cell death. As shown in Figure 4B, we first confirmed siRNA knockdown of PARP14 in HepG2 cells indeed caused activation of JNK1 phosphorylation and apparent formation of cleaved PARP1 (a hallmark of apoptosis). Treatment of the cells by **H10** or **AD3** caused similar effects at as low as 10 μM, indicating that both compounds were able to chemically knockdown endogenous PARP14 activities effectively. Subsequent caspase-3/7-mediated cell apoptosis was confirmed by FACS, in vitro caspase-3 enzymatic assay, and Western blotting analysis (Figures 4C and S17). Similar apoptosis was also detected in compound-treated RPMI-8226 cells (a myeloma cell line). Finally, we carried out combination drug treatment experiments by treating the cells with **H10**/**AD3** and another well-known drug (doxorubicin (DOX) for HepG2 and dexamethasone (DEX) for RPMI-8226 cells, respectively). Both DOX and DEX are anticancer agents. As shown in Fig-

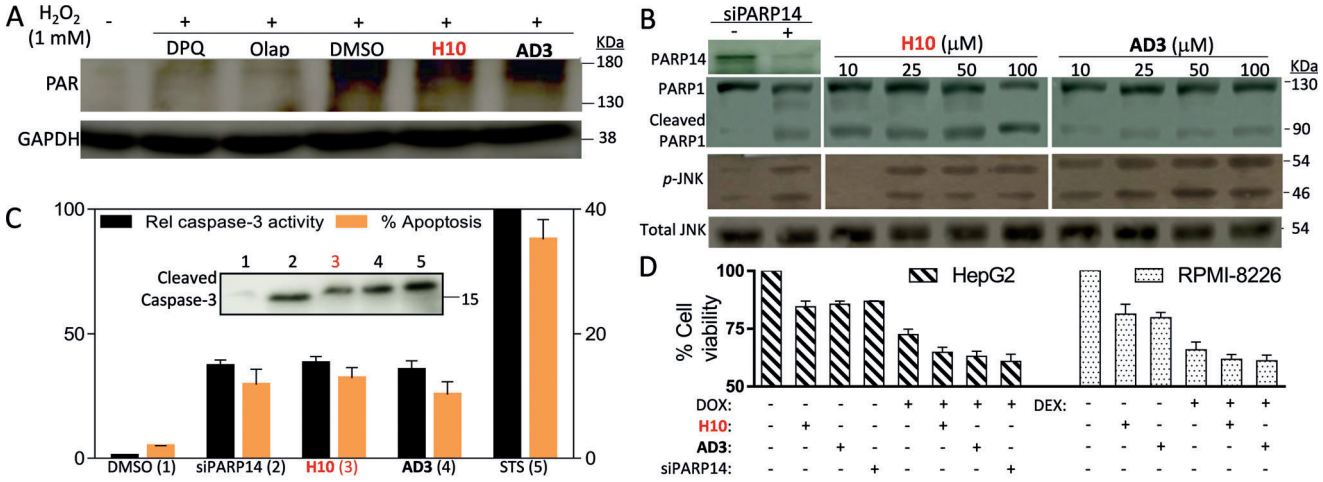

Figure 4. A) H_2O_2-induced PAR formation (1 mM, 1 h) of HepG2 cells were inhibited by PARP1 inhibitors (10 and 1 μM for DPQ and Olaparib, respectively), but not **H10**/**AD3** (25 μM). B) Effects of PARP14 knockdown (siPARP14, 10–100 μM of **H10** or **AD3**) in HepG2 include promotion of PARP1 cleavage and JNK1 phosphorylation. C) Caspase-3-activated apoptosis of HepG2 cells was observed as a result of PARP14-knockdown in (B), determined by in vitro caspase-3 enzymatic assay (black bars) and FACS (orange bars). A positive control was done with cells treated with staurosporine (STS, 200 nM). The concentration of **H10**/**AD3** was 100 μM. Inset: WB analysis with anti-cleaved caspase-3 Ab. D) XTT cell viability results showing effects of combination drug treatments with doxorubicin (DOX)-treated HepG2 and dexamethasone (DEX)-treated RPMI-8226 cells in the presence of **H10**/**AD3** (25 μM). The Dox/DEX concentration was 10 μM.

ure 4 D, both of the PARP14 inhibitors showed enhanced cell-killing properties in the presence of DOX or DEX, respectively, similar to what was observed from the corresponding siRNA experiments, as well as previous reports.[4,5] All of these lines of evidence thus confirmed **H10** and **AD3** are the first-ever in situ-active PARP14 inhibitors capable of blocking endogenous PARP14 activities in both tumor cell lines.

In conclusion, by using on-chip CuAAC, we have developed a small molecule microarray capable of rapid synthesis and screening of potential PARP inhibitors. The successful discovery of **H10**, a potent and selective PARP14 inhibitor that showed moderate inhibitory properties against endogenous PARP14 in different tumor cells, indicates this microarray-based strategy might be amenable for the future discovery of selective inhibitors against other PARP proteins. The X-ray structure of PARP14/**H10** also unequivocally established the bidentate binding mode of **H10** for the first time.

Coordinates and structure factors have been deposited in the Protein Data Bank (PARP14-**H5**, PDB entry 5LXP; PARP14-**H10**, PDB entry 5LYH).

Acknowledgments

Funding was provided by the National Medical Research Council (CBRG/0038/2013), Ministry of Education (MOE2013-T2-1–048) of Singapore, the IngaBritt & Arne Lundberg Foundation, the Swedish Cancer Society, the Swedish Research Council, and the European Community's Seventh Framework Programme (FP7/2007–2013) under BioStruct-X (grant agreement No. 283570). We thank the Protein Science Facility at Karolinska Institute for technical support, Joseph Brock for help with synchrotron data collection and the beamline staff at DIAMOND (Didcot, UK) and PETRA (Hamburg, Germany) for assistance.

Conflict of interest

The authors declare no conflict of interest.

Keywords: click chemistry · high-throughput screening · microarrays · PARP inhibitors · X-ray crystallography

[1] B. A. Gibson, W. L. Kraus, *Nat. Rev. Mol. Cell Biol.* **2012**, *13*, 411–424.
[2] L. Virag, C. Szabo, *Pharmacol. Rev.* **2002**, *54*, 375–429.
[3] E. Wahlberg, T. Karlberg, E. Kouznetsova, N. Markova, A. Macchiarulo, A. G. Thorsell, E. Pol, A. Frostell, T. Ekblad, D. Oncu, B. Kull, G. M. Robertson, R. Pellicciari, H. Schuler, J. Weigelt, *Nat. Biotechnol.* **2012**, *30*, 283–288.
[4] A. Barbarulo, V. Iansante, A. Chaidos, K. Naresh, A. Rahemtulla, G. Franzoso, A. Karadimitris, D. O. Haskard, S. Papa, C. Bubici, *Oncogene* **2013**, *32*, 4231–4242.
[5] V. Iansante, P. M. Choy, S. W. Fung, Y. Liu, J. G. Chai, J. Dyson, A. Del Rio, C. D'Santos, R. Williams, S. Chokshi, R. A. Anders, C. Bubici, S. Papa, *Nat. Commun.* **2015**, *6*, 7882.
[6] C. D. Andersson, T. Karlberg, T. Ekblad, A. E. Lindgren, A. G. Thorsell, S. Spjut, U. Uciechowska, M. S. Niemiec, P. Wittung-Stafshede, J. Weigelt, M. Elofsson, H. Schuler, A. Linusson, *J. Med. Chem.* **2012**, *55*, 7706–7718.
[7] T. Ekblad, A. E. Lindgren, C. D. Andersson, R. Caraballo, A. G. Thorsell, T. Karlberg, S. Spjut, A. Linusson, H. Schuler, M. Elofsson, *Eur. J. Med. Chem.* **2015**, *95*, 546–551.
[8] D. V. Ferraris, *J. Med. Chem.* **2010**, *53*, 4561–4584.
[9] Z. Na, B. Peng, S. Ng, S. Pan, J. S. Lee, H. M. Shen, S. Q. Yao, *Angew. Chem. Int. Ed.* **2015**, *54*, 2515–2519; *Angew. Chem.* **2015**, *127*, 2545–2549.

[10] C. M. Gower, M. E. K. Chang, D. J. Maly, *Crit. Rev. Biochem. Mol. Biol.* **2014**, *49*, 102 – 115.
[11] R. Srinivasan, M. Uttamchandani, S. Q. Yao, *Org. Lett.* **2006**, *8*, 713 – 716.
[12] a) M. D. Shultz, et al., *J. Med. Chem.* **2012**, *55*, 1127 – 1136; b) T. Haikarainen, M. Narwal, P. Joensuu, L. Lehtio, *ACS. Med. Chem. Lett.* **2014**, *5*, 18 – 22; c) J. W. Johannes, et al., *ACS Med. Chem. Lett.* **2015**, *6*, 254 – 259.
[13] R. Srinivasan, J. Li, S. L. Ng, K. A. Kalesh, S. Q. Yao, *Nat. Protoc.* **2007**, *2*, 2655 – 2664.
[14] X. S. Wang, B. S. Huang, X. Y. Liu, P. Zhan, *Drug Discovery Today* **2016**, *21*, 118 – 132.
[15] J. A. Hong, D. V. Neel, D. Wassaf, F. Caballero, A. N. Koehler, *Curr. Opin. Chem. Biol.* **2014**, *18*, 21 – 28.
[16] a) Z. Na, S. Pan, M. Uttamchandani, S. Q. Yao, *Angew. Chem. Int. Ed.* **2014**, *53*, 8421 – 8426; *Angew. Chem.* **2014**, *126*, 8561 – 8566; b) C. J. Zhang, C. Y. Tan, J. Ge, Z. Na, G. Y. Chen, M. Uttamchandani, H. Sun, S. Q. Yao, *Angew. Chem. Int. Ed.* **2013**, *52*, 14060 – 14064; *Angew. Chem.* **2013**, *125*, 14310 – 14314; c) H. Wu, J. Ge, P.-Y. Yang, J. Wang, M. Uttamchandani, S. Q. Yao, *J. Am. Chem. Soc.* **2011**, *133*, 1946 – 1954; d) M. Uttamchandani, W. L. Lee, J. Wang, S. Q. Yao, *J. Am. Chem. Soc.* **2007**, *129*, 13110 – 13117.
[17] C. D. Rillahan, E. Schwartz, C. Rademacher, R. McBride, J. Rangarajan, V. V. Fokin, J. C. Paulson, *ACS Chem. Biol.* **2013**, *8*, 1417 – 1422.
[18] a) R. Srinivasan, L. P. Tan, H. Wu, P.-Y. Yang, K. A. Kalesh, S. Q. Yao, *Org. Biol. Chem.* **2009**, *7*, 1821 – 1828; b) Z. Li, P. Hao, L. Li, C. Y. Tan, X. Cheng, G. Y. Chen, S. K. Sze, H. M. Shen, S. Q. Yao, *Angew. Chem. Int. Ed.* **2013**, *52*, 8551 – 8556; *Angew. Chem.* **2013**, *125*, 8713 – 8718.
[19] M. R. Purnell, W. J. Whish, *Biochem. J.* **1980**, *185*, 775 – 777.
[20] P. Y. Wang, J. Li, X. Jiang, Z. Q. Liu, N. Ye, Y. J. Xu, G. F. Yang, Y. C. Xu, A. Zhang, *Tetrahedron* **2014**, *70*, 5666 – 5673.
[21] H. Venkannagari, P. Verheugd, J. Koivunen, T. Haikarainen, E. Obaji, Y. Ashok, M. Narwal, T. Pihlajaniemi, B. Lüscher, L. Lehtiö, *Cell Chem. Biol.* **2016**, *23*, 1251 – 1260.

Manuscript received: October 2, 2016
Revised: November 22, 2016
Final Article published: ■■ ■■, ■■■■

Communications

High-Throughput Screening

B. Peng, A.-G. Thorsell, T. Karlberg, H. Schüler,* S. Q. Yao* ——— ▮▮▮▮–▮▮▮▮

Small Molecule Microarray Based Discovery of PARP14 Inhibitors

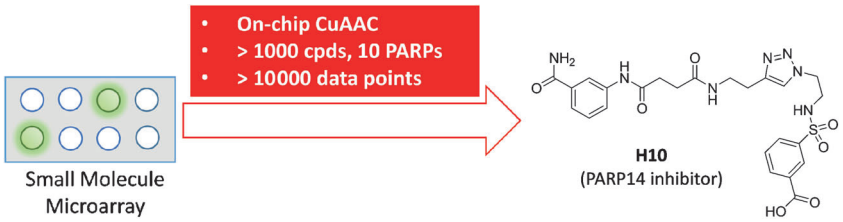

"Spotting" the Hit: A small molecule microarray was developed for miniaturized on-chip synthesis and screening of >1000 potential bidentate inhibitors against poly(ADP-ribose) polymerases (PARPs), which led to the successful discovery of a potent PARP14 bidentate inhibitor (IC_{50} = 0.49 μM) with >20-fold selectivity over PARP1.